

# CMOS-compatible dual-output silicon modulator for analog signal processing

S. J. Spector<sup>1\*</sup>, M. W. Geis<sup>1</sup>, G.-R. Zhou<sup>2</sup>, M. E. Grein<sup>1</sup>, F. Gan<sup>2</sup>, M.A. Popović<sup>2</sup>, J. U. Yoon<sup>1</sup>, D. M. Lennon<sup>1</sup>, E. P. Ippen<sup>2</sup>, F. X. Kärtner<sup>2</sup> and T. M. Lyszczarz<sup>1</sup>

<sup>1</sup>Lincoln Laboratory, Massachusetts Institute of Technology, Lexington, MA 02420

<sup>2</sup>Massachusetts Institute of Technology, Cambridge, MA 02139

\*[spector@ll.mit.edu](mailto:spector@ll.mit.edu)

**Abstract:** A broadband, Mach-Zehnder-interferometer based silicon optical modulator is demonstrated, with an electrical bandwidth of 26 GHz and  $V_{\pi}L$  of 4 V·cm. The design of this modulator does not require epitaxial overgrowth and is therefore simpler to fabricate than previous devices with similar performance.

©2008 Optical Society of America

**OCIS codes:** (250.7360) Waveguide modulators; (230.2090) Electro-optical devices; (130.3120) Integrated optics devices.

---

## References and links

1. G. T. Reed, and A. P. Knights, "Silicon Photonics: an Introduction," (John Wiley, Chichester, 2004)
2. L. Liao, A. Liu, D. Rubin, J. Basak, Y. Chetrit, H. Nguyen, R. Cohen, N. Izhaky, and M. Paniccia, "40 Gbit/s silicon optical modulator for high-speed applications," *Electron. Lett.*, **43** (22) pp. 1196-1197 (2007).
3. Q. Xu, S. Manapatruni, B. Schmidt, J. Shakya, and M. Lipson, "12.5 Gbit/s carrier-injection-based silicon microring silicon modulators," *Opt. Express* **15**, 430-436 (2007).
4. L. Liao, D. Samara-Rubio, M. Morse, A. Liu, and D. Hodge, "High speed silicon Mach-Zehnder modulator," *Opt. Express* **13**, 3129-3135 (2005).
5. R. A. Soref, and B. R. Bennett, "Electrooptical effects in silicon," *IEEE J. Quantum Electron.* **23**, 123-129 (1987).
6. D. Marris-Morini, L. Vivien, J. M. Fédéli, E. Cassan, P. Lyan, and S. Laval, "Low loss and high speed silicon optical modulator based on a lateral carrier depletion structure," *Opt. Express* **16**, 334-339 (2008).
7. J. C. Twichell, and R. Helkey, "Phase-encoded optical sampling for analog-to-digital converters," *IEEE Photonic Technol. Lett.* **12**, 1237-1239 (2000).
8. F. X. Kärtner, R. Amatya, M. Araghchini, J. Birge, H. Byun, J. Chen, M. Dahlem, N. A. DiLello, F. Gan, C. W. Holzwarth, J. L. Hoyt, E. P. Ippen, A. Khilo, J. Kim, M. Kim, A. Motamedi, J. S. Orcutt, M. Park, M. Perrott, M. A. Popović, R. J. Ram, H. I. Smith, G. R. Zhou, S. J. Spector, T. M. Lyszczarz, M. W. Geis, D. M. Lennon, J. U. Yoon, M. E. Grein, and R. T. Schulein, "Photonic Analog-to-Digital Conversion with Electronic-Photonic Integrated Circuits," *Proceedings of SPIE Photonics West*, (Invited Paper), San Jose, CA, USA, Jan. 2008.
9. K. Solehmainen, M. Kapulainen, M. Harjanne, and T. Aalto, "Adiabatic and multimode interference couplers on silicon-on-insulator," *IEEE Photonic Technol. Lett.* **18**, 2287-2289 (2006).
10. T. Shoji, T. Tsuchizawa, T. Watanabe, K. Yamada, and H. Morita, "Spot-size converter for low-loss coupling between 0.3- $\mu\text{m}$ -square Si wire waveguides and single-mode fibers," *EOS 2002. 2002 IEEE/LEOS Annual Meeting Conference Proceedings*, 1, pp. 289-290.
11. P. W. Juodawlkis, J. C. Twichell, G. E. Betts, J. J. Hargreaves, R. D. Younger, J. L. Wasserman, F. J. O'Donnell, K. G. Ray, and R. C. Williamson, "Optically Sampled Analog-to-Digital Converters," *IEEE Trans. On Microwave Theory and Tech.* **49**, 1840-1853 (2001).

---

## 1. Introduction

The development of silicon based photonics has the potential to allow monolithically-integrated, low-cost optical devices on a platform compatible with CMOS circuits [1]. Optical modulators are an essential component in most applications, and there has been considerable recent effort directed at developing silicon based optical modulators [2-4]. The most successful devices have used the free-carrier plasma dispersion effect [5], where a change in density of carriers causes a change in the refractive index of silicon. This effect can be accessed by carrier injection in a p-i-n diode [3], accumulation in a MOS capacitor [4], or

carrier depletion in a p-n diode [2]. Carrier depletion has achieved the best high speed result to date, with a Mach Zehnder based modulator achieving 30 GHz of electrical bandwidth and a  $V_{\pi}L$  of 4 V·cm [2]. One disadvantage of the design in [2] is the use of a top contact which requires an epitaxial silicon overgrowth. A recent result used a design that eliminated the top contact, but did not achieve the same performance [6]. The design described here does not use a top contact, and shows performance approaching that of [2]. The modulator demonstrated here achieves 26 GHz of electrical bandwidth and a  $V_{\pi}L$  of 4 V·cm.

There are additional considerations for the design of a modulator which may depend on the application. For analog applications, a modulator with two complementary outputs can be used to linearize the transfer function of the modulator and compensate for fluctuations external to the modulator [7,8], such as variations in the laser output. The design described here uses a balanced Mach-Zehnder interferometer with broadband 3 dB couplers. The input 3 dB coupler is a symmetric Y-junction, while the output 3 dB coupler uses an adiabatic 4-port structure to provide two complementary outputs.

## 2. Design

The modulators are fabricated using Unibond silicon-on-insulator (SOI) wafers with a 0.22  $\mu\text{m}$  thick layer of silicon above a 3  $\mu\text{m}$  buried oxide. Figure 1(a) schematically shows the top-view of the modulator. The active areas of the device are p-n diode phase shifter sections in the arms of the modulator. Modulators using reverse bias p-n junctions can be very fast; their electrical speed is usually only limited by capacitance. By employing a relatively short interaction length of 0.5 mm (the travel time of the light is only 5 ps), a simple lumped-element electrode design can be used to achieve speeds of about 30 GHz. The modulator can be operated in a push-pull configuration by driving the center electrode (as shown), or a single arm can be driven. An additional thermal phase shifter (not shown) is fabricated on one arm, to allow the relative optical phase of the two arms of the modulator to be adjusted independently of the diodes.

An adiabatic 4-port 3 dB coupler is used to interfere the two arms at the output of the Mach-Zehnder interferometer leading to two complementary modulator output ports. An adiabatic 3 dB coupler design [9] was chosen over a conventional 3 dB coupler because the former has less stringent fabrication tolerances. Typically, adiabatic couplers have the disadvantage that they are fairly large – in the millimeters. This is not the case in strongly confined waveguides, however. Here an effort was made to optimize the design for short length, and the resulting design for the adiabatic coupler is only 130  $\mu\text{m}$  long. Mode-profile converting tapers are also needed to provide efficient fiber-to-chip coupling at the input and outputs. For this purpose, a silicon inverse-taper mode converter combined with a lower index silicon oxynitride waveguide [10] was used.

Figure 1(b) shows schematically the cross-section of the waveguide in the active area of the modulator. The central region (core) of the waveguide is 220 nm thick, 500 nm wide, and lightly n-type doped to a concentration of  $2 \times 10^{17} \text{ cm}^{-3}$ , resulting in a break down voltage of 16 V. The sidewalls are moderately doped, n-type on one side and p-type on the other, to a concentration of  $10^{18} \text{ cm}^{-3}$  and an approximate depth of 50 nm. When a reverse bias is applied, a depletion region forms at the p-n junction on one side of the waveguide. This depletion region's lateral size increases into the center of the waveguide as the bias is increased, creating a change in the refractive index of the waveguide. To make electrical contact to the core of the waveguide, heavily doped, ( $10^{19} \text{ cm}^{-3}$  concentration), 50 nm thick slab regions connect the waveguide to metal contacts located 1  $\mu\text{m}$  away. To ensure good ohmic contact, the silicon slab under the metal contacts is degenerately doped to a concentration of  $10^{21} \text{ cm}^{-3}$ . The parasitic resistance of the diodes including ohmic contacts and the resistance of the doped Si is usually  $<0.3 \Omega/\text{cm}$ .

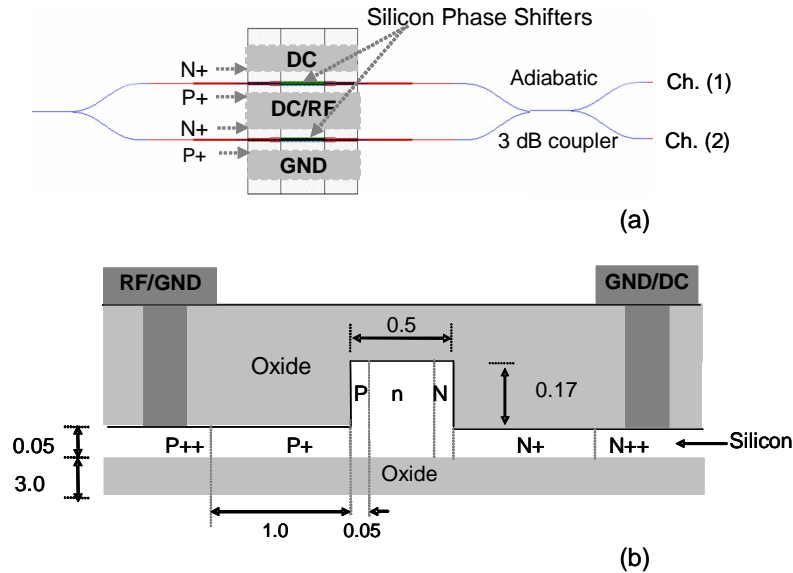


Fig. 1. (a) Top-view layout of the dual-output modulator. (b) Schematic view of the cross-section of one of the phase shifters. (All dimensions are in  $\mu\text{m}$ ).

### 3. Modeling

To model the carrier concentration in the waveguide, numerical simulations were performed by solving Poisson and carrier continuity equations. The modeled change in carrier concentration determines a change in the material index of silicon which can then be used to determine the change in the modal index,  $N_{\text{eff}}$ . The simulations show that the application of a reverse bias of 8 V causes an increase in the modal index,  $\Delta N_{\text{eff}}$ , of  $\sim 1.67 \times 10^{-4}$  as well as in the absorption coefficient,  $\Delta \alpha$ , of  $\sim 1.61 \text{ cm}^{-1}$ . With an interaction length of 0.5 mm, this corresponds to a phase change  $\Delta \phi$  of  $0.11\pi$  and absorption loss of 0.34 dB.

Simple modeling can be used to estimate the electrical bandwidth of a 0.5 mm long device. The input capacitance of the diodes in the Mach Zehnder interferometer is calculated to be  $\sim 0.1 \text{ pF}$  and the contact pad capacitance is  $< 0.05 \text{ pF}$ . This gives an estimate total capacitance from 0.1 and 0.15 pF. The  $5 \Omega$  of internal resistance in the Mach Zehnder and  $50 \Omega$  output impedance of the RF power supply, gives a calculated RC bandwidth of between 20 and 30 GHz.

### 4. Results

The DC response of the modulator was tested by varying the DC bias voltage on arm #1 while the other arm remained at the same bias level. Figure 2 shows the simulated and measured normalized light intensity as a function of the applied voltage, for the two complementary outputs. The measured and simulated results are in good agreement with each other. To get a better measure of  $V_{\pi}L$ , a longer device, with 5 mm arm lengths, was also measured. The output of that modulator (which was fabricated with only one output channel) is also shown in Fig. 2, and gives a  $V_{\pi}L$  of just over 4 V·cm. This is comparable to what had been achieved earlier with a structure requiring more complicated fabrication [2]. Operating the modulator in a push-pull configuration has also been demonstrated, and cuts the effective  $V_{\pi}L$  for the device in half to 2 V·cm, as expected.

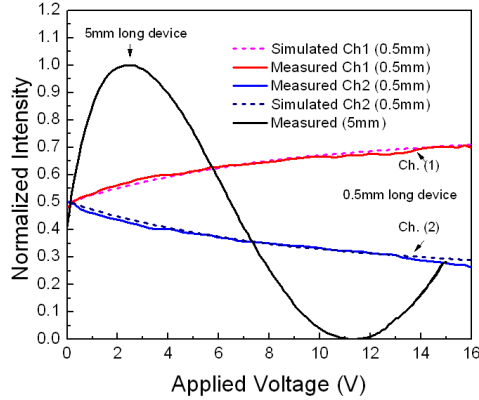


Fig. 2. Measured and simulated normalized light transmission as a function of applied voltage.

The high-frequency response of the modulator was measured by the following experimental setup: a 1550 nm laser beam is amplified and coupled into the modulator chip via a lensed fiber. The output beam from the modulator chip is collected by an aspheric lens, goes through a fiber amplifier and a 2 nm bandpass filter, and is finally detected with a ~50 GHz InGaAs photodetector. A network analyzer is used to drive the modulator and to measure the signal on the photodetector. In order to distinguish the bandwidth limiting effects associated with cabling from the actual bandwidth performance of the device, the RF transmission response is first measured through the cables only. The cables were found to have a 3 dB bandwidth of 10 GHz. Then the fabricated modulator device is connected with the same cables to measure the total response. The net performance of the device is then obtained by subtracting the measured cable response from the total response. No attempt was made to impedance match the Mach Zehnder modulator to the 50- $\Omega$  impedance of the RF source. Any losses from this impedance mismatch are not measured or compensated by this method.

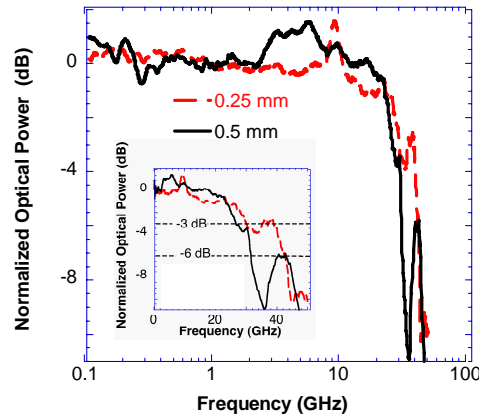


Fig. 3. Measured frequency response of the modulator.

Figure 3 shows the small signal frequency response of the modulator after correction for frequency dependent cable losses. A 3-dB cut-off frequency of 26 GHz is reached in a 0.5 mm device, which agrees with the estimate calculated above. A shorter device with 0.25 mm long phase shifters was also measured, and exhibits between 30-40 GHz of bandwidth. In addition to the RC limitation mentioned above, the electrode can no longer be considered a lumped-element device at high frequencies. This leads to unpredictable behavior at higher frequencies, such as a secondary peak at 40 GHz in the 0.5 mm device. In order to drive the modulator with higher power, an RF amplifier and bias-T were added to the above

experimental set-up. When running the 0.5 mm device in a push-pull configuration, 46 mW of RF power achieves ~22% modulation depth, as defined by [11], for a 26 GHz sinusoid. The RF power was measured by replacing the modulator with the network analyzer.

From the  $V\pi L$  of 2 V·cm, it can be calculated that a voltage of  $\pm 4.5$  V is necessary to achieve a 22% modulation depth in a 0.5 mm device. This is roughly twice the voltage of a 46 mW signal into a 50  $\Omega$  load. This difference can be explained by an enhancement of the drive voltage due to the impedance mismatch at the modulator. The modulator is expected to have high impedance, which causes most of the drive signal to be reflected. The combination of the reflected signal with the forward signal doubles the voltage at the modulator.

The optical loss of the device was estimated to be 5dB from the total fiber to fiber loss of 10 dB.

## 5. Discussion

The measured 22% modulation depth is small, but sufficient for some applications. In an optically sampled analog to digital converter, this modulation depth is sufficient to achieve a signal to noise ratio of 47 dB [11]. This is only 6 dB less than the theoretical maximum of 53 dB achieved with a 50% modulation depth under otherwise similar conditions.

The modulation depth could also be improved by going to a traveling-wave electrode design. A traveling-wave electrode would allow devices to have longer lengths, and therefore lower  $V\pi$ , while still achieving high-speed operation. The results on the 0.25 mm device indicate that 40 GHz of bandwidth should be feasible in longer devices if a traveling-wave electrode is used. In addition, modeling has indicated that changing the doping type from n-type to p-type in the center of the waveguide can potentially increase the modulation efficiency by a factor of 2~3, thereby reaching a  $V\pi L$  of 2 V·cm.

## 6. Conclusion

We have demonstrated a silicon modulator with two complementary outputs, a  $V\pi L$  of 4 V·cm (or 2 V·cm for the whole device operating in push-pull), and a 3-dB bandwidth of 26 GHz. A modulation depth of 22% was achieved. The insertion loss of the device is 10 dB, about half of which occurs on chip, and half of which occurs coupling in and out of the device.

## Acknowledgements

Gui-Rong Zhou is grateful to the Natural Science Engineering Research Council of Canada (NSERC) for support by a postdoctoral fellowship. The Lincoln Laboratory portion of this work was sponsored by the EPIC Program of the Defense Advanced Research Projects Agency under Air Force Contract FA8721-05-C-0002. The work on MIT Campus was sponsored by the DARPA EPIC Program under contract W911NF-04-1-0431. Opinions, interpretations, conclusions, and recommendations are those of the authors, and do not necessarily represent the view of the United States Government.